Inhibition of Thermolysin by Phosphonamidate Transition-State Analogues: Measurement of ^{31}P–^{15}N Bond Lengths and Chemical Shifts in Two Enzyme–Inhibitor Complexes by Solid-State Nuclear Magnetic Resonance†

Valérie Copié,‡ Andrew C. Kolbert,‡ David H. Drewry,§ Paul A. Bartlett,§ Terrence G. Oas,∥ and Robert G. Griffin*,‡

Francis Bitter National Magnet Laboratory and Department of Chemistry, Massachusetts Institute of Technology, Cambridge, Massachusetts 02139, Whitehead Institute for Biomedical Research, Massachusetts Institute of Technology, Cambridge, Massachusetts 02139, and Department of Chemistry, University of California, Berkeley, California 94720

Received February 12, 1990; Revised Manuscript Received May 30, 1990

ABSTRACT: ^{31}P and ^{15}N chemical shifts and ^{31}P–^{15}N bond lengths have been measured with solid-state NMR techniques in two inhibitors of thermolysin, carbobenzoxy-Gly^{P}-L-Leu-L-Ala (ZG^{P}LA) and carbobenzoxy-L-Phe^{P}-L-Leu-L-Ala (ZF^{P}LA), both as free lithium salts and when bound to the enzyme. Binding of both inhibitors to thermolysin results in large changes in the ^{31}P chemical shifts. These changes are more dramatic for the tighter binding inhibitor ZF^{P}LA, where a ~20 ppm downfield movement of the ^{31}P isotropic chemical shift (σ_{iso}) is observed. This shift is due to changes in the shift tensor elements σ_{11} and σ_{22}, while σ_{33} remains essentially constant. We observed a similar pattern for ZG^{P}LA, but only a ~5 ppm change occurs in σ_{iso}. The changes in the ^{15}N chemical shifts for both inhibitors are small upon binding, amounting to downfield shifts of 2 and 4 ppm for ZG^{P}LA and ZF^{P}LA, respectively. This indicates that there are no changes in the protonation state of the ^{15}N in either the ZF^{P}LA– or the ZG^{P}LA–thermolysin complex. NMR distance measurements yield a P–N bond length r_{P-N} = 1.68 ± 0.03 Å for the tight binding inhibitor ZF^{P}LA both in its free lithium salt form and in its thermolysin–ZF^{P}LA complex, a distance that is much shorter than the 1.90-Å distance reported by X-ray crystallography studies [Holden et al. (1987) *Biochemistry 26*, 8542–8553]. For the ZG^{P}LA inhibitor, we measure r_{P-N} = 1.60 ± 0.05 Å, a distance which, within the experimental errors of our measurements, we consider to be similar to that of ZF^{P}LA. Moreover, we observe no change in P–N bond length upon binding of ZG^{P}LA to thermolysin. It is clear that the large changes in ^{31}P chemical shift observed in the thermolysin–ZF^{P}LA complex are not correlated with changes in either the ^{15}N protonation state or P–N bond length. The ^{31}P NMR data suggest that the tight binding of ZF^{P}LA may be due to the formation of a strong bidentate complex between the inhibitor's phosphorus oxygen atoms and the protein zinc ion, and/or to favorable hydrophobic interactions between the inhibitor and the enzyme active site.

Thermolysin is a thermostable zinc-containing endopeptidase of molecular weight 34 600 isolated from the thermophilic bacterium *Bacillus thermoproteolyticus* (Endo, 1962). Related peptidases, such as the angiotensin converting enzyme, enkephalinase, collagenase, and other neutral endopeptidases, have been recognized to play important roles in cellular and hormonal metabolism. Hence, their mode of action and the discovery of inhibitors have been of interest in the development of pharmaceutical agents (Ehlers et al., 1989; Erdos et al., 1989; Fournie-Zaluski, 1988; Johnson et al., 1987; Haslanger et al., 1989; Seymour et al., 1989).

In order to understand the catalytic mechanism of thermolysin, its crystal structure has been determined to 1.60-Å resolution (Holmes & Matthews, 1982) and indicates that the protein consists mainly of two spherical domains with a deep cleft in the middle of the molecule, which constitutes the active site. Additional X-ray studies of a number of enzyme–inhibitor complexes have been performed (Holmes & Matthews, 1981, 1983; Kester & Matthews, 1977; Weaver & Matthews, 1977; Holden & Matthews, 1988; Bolognesi & Matthews, 1979; Monzingo & Matthews, 1984) together with computer modeling of potential intermediates and transition states along the reaction pathway (Hangauer et al., 1984). These investigations have led to a model for the binding of extended substrates to thermolysin, and a mechanism in which Glu-143 acts as a general base to promote the attack of a water molecule on the carbonyl carbon of the scissile peptide bond. Following this step, protonation of the peptide nitrogen leads to a zwitterionic tetrahedral intermediate, as shown in Figure 1, where the hydrated carbonyl and three protein ligands form a pentacoordinated zinc ion. The next step envisaged in this mechanism is the collapse of the tetrahedral intermediate and cleavage of the C–N bond.

The concept of transition-state analogues has been very useful in designing potent enzyme inhibitors (Wolfenden, 1976; Wolfenden & Frick, 1987). Such transition-state analogues are designed on the assumption that structures which mimic the normal transition state have optimal interactions with the enzyme at that site (Pauling, 1946; Wolfenden, 1976). During catalyis favorable binding interactions, not available to the ground-state enzyme–substrate complex, develop as the enzyme–substrate transition-state complex forms. These enhanced binding interactions assist in lowering the activation energy of the reaction, and hence in accelerating the enzymatic rate (Jencks, 1975, 1980, 1981). Transition-state analogue

† This research was supported by the National Institutes of Health (GM-23403, CA-22747, RR-00995). T.G.O. is a recipient of an American Cancer Society Postdoctoral Fellowship (PF-2949).

* To whom correspondence should be addressed.

‡ Francis Bitter National Magnet Laboratory and Department of Chemistry, Massachusetts Institute of Technology.

§ University of California.

∥ Whitehead Institute for Biomedical Research, Massachusetts Institute of Technology.

0006-2960/90/0429-9176$02.50/0

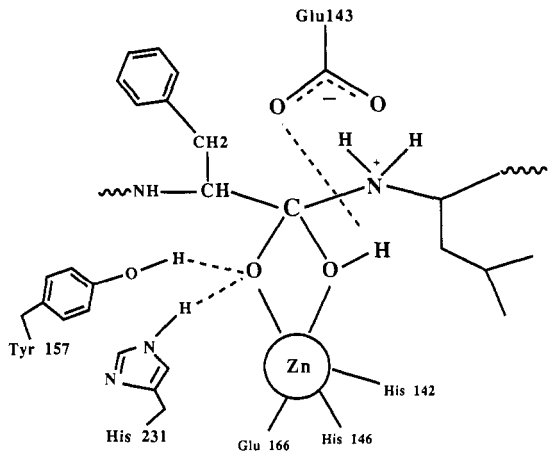

FIGURE 1: Schematic illustration of the postulated tetrahedral intermediate structure formed during thermolysin's enzymatic reaction. Presumed hydrogen bond interactions are drawn as dashed lines. Thermolysin's zinc ion is shown coordinated to three protein amino acid residues and two substrate ligands.

inhibitors take advantage of these additional interactions by possessing, in their stable structures, key structural elements of the unstable enzyme–substrate transition-state complex (Jencks, 1987; Fersht, 1984).

Recently, very potent inhibitors of thermolysin have been synthesized in which the scissile peptide linkage has been replaced by a tetrahedral phosphorus ester or amide moiety (phosphonate and phosphonamidate inhibitors, respectively) (Bartlett & Marlowe 1983, 1987a,b). K_i values for a series of phosphonamidate tripeptide inhibitors show a strong correlation with the K_m/k_{cat} of the corresponding substrates as expected for transition-state analogues (Bartlett & Marlowe, 1983; Wolfenden, 1976). A number of these phosphonamidate inhibitors have been bound to crystalline thermolysin, and the crystal structures of the enzyme–inhibitor complexes have been determined (Tronrud et al., 1986, 1987; Holden et al., 1987). From these X-ray crystallographic studies, it has been postulated that the tightest binding inhibitors are the ones which (1) have optimal interactions with the enzyme amino acid residues in hydrophobic clefts, (2) can form a tight bidentate complex with thermolysin's zinc ion, and (3) possess a long P–N bond and a reduced P–N–C bond angle. These features are consistent with the structure for the enzyme–substrate transition-state described earlier, where cleavage of the C–N bond and protonation of the amide nitrogen occur concurrently (Figure 1). Thus, for the tightest binding inhibitor, ZF^{P}LA, with a K_i value equal to 0.068 nM, the X-ray data suggest that, in the ZF^{P}LA–thermolysin complex, the amide nitrogen is protonated and that the P–N bond is lengthened to a distance of ~1.9 Å (Holden et al., 1987).

One technique that can be used to investigate the proposed correlation between the tightness of binding of phosphonamidate inhibitors and P–N bond length is solid-state NMR.[1] Bond length information may be obtained by measuring the direct dipolar coupling between spin pairs such as ^{31}P–^{15}N, which is proportional to $1/r^3$, where r is the internuclear distance (Abragam, 1961). This is most readily accomplished with two-dimensional MAS dipolar–chemical shift techniques

[1] Abbreviations: CP, cross-polarization; CSA, chemical shift anisotropy; FID, free induction decay; MAS, magic angle spinning; NMR, nuclear magnetic resonance; TMP, trimethyl phosphite; ZG^{P}LA, carbobenzoxy-Gly^P-L-leucyl-L-alanine; ZF^{P}LA, carbobenzoxy-Phe^P-L-leucyl-L-alanine. X^P is used to indicate that the trigonal carbon of the normal peptide substrate has been replaced by the tetrahedral phosphorus of a phosphonamidate group in the thermolysin inhibitors.

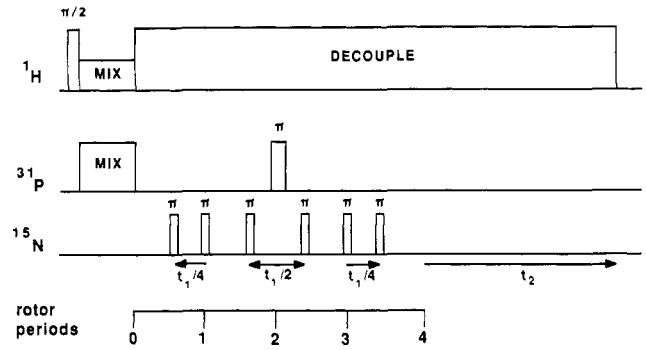

FIGURE 2: Pulse sequence for XDMR4. The ^{15}N π pulses move in the direction of the arrows for different values of t_1, maintaining the same constant $4N$ rotor periods prior to detection in each case. Acquisition begins on the ^{31}P channel at $4\tau_r$.

which contain a dipolar evolution period followed by detection of the usual chemical shift free induction decay (FID). With this approach it has been possible to measure accurately dipolar couplings in polycrystalline samples containing strongly coupled spin pairs such as ^{13}C–^{1}H, even in the presence of large shielding anisotropies (Munowitz et al., 1981; Munowitz & Griffin, 1982; Roberts et al., 1987). The dipolar spectrum is extracted from the two-dimensional landscape by coadding slices parallel to the ω_1 axis. The sideband intensities from this ω_1 "projection" may then be compared with the results of numerical simulations to obtain the dipolar coupling and, therefore, the bond length. For greatest accuracy, however, these experiments require sample spinning speeds less than the size of the coupling being measured. Since ^{31}P–^{15}N dipolar couplings are weak (~1 kHz), speeds of approximately 500 Hz are appropriate. At the moment these slow speeds are technically difficult to achieve for extended periods. Furthermore, the two-dimensional spectrum obtained from the usual dipolar–chemical shift experiment (Munowitz & Griffin, 1982) is overwhelmed by the large number of chemical shift sidebands in the ω_2 dimension, thus reducing the sensitivity of the spectrum and complicating the analysis.

Recently, a number of one- and two-dimensional techniques have been developed which enhance the effects of small dipolar couplings, permitting their measurement at high spinning speeds (Oas et al., 1988; Levitt et al., 1988; Kolbert et al., 1989; Gullion & Schaefer, 1988, 1989a,b). The physical basis for the two-dimensional experiments is the introduction of π pulses which interfere with rotational echo formation (Olejniczak et al., 1984). When π pulses are present during the t_1 dipolar evolution period, they result in an *effective* reduction of the spinning speed, $\omega_r/2\pi$, in the ω_1 dimension by a factor of 2–5.

In this study, we utilize the two-dimensional XDMR4 experiment developed by Gullion and Schaefer (1988), illustrated in Figure 2, which achieves an effective reduction in $\omega_r/2\pi$ by a factor of 5. After the preparation of transverse magnetization by cross-polarization (Pines et al., 1973), a series of π pulses are applied at the ^{15}N and ^{31}P frequencies over a constant $4N$ rotor periods, $\tau_r = 2\pi/\omega_r$. The π pulses at τ_r, $2\tau_r$, and $3\tau_r$ are stationary, while the others move in the directions indicated for different values of t_1, maintaining the same constant time prior to acquisition in each case. The usual chemical shift FID is detected during t_2. With this experiment, ^{31}P–^{15}N dipolar couplings of less than 1 kHz in magnitude can be measured at *actual* spinning speeds exceeding this value by more than a factor of 2.

In this paper we report solid-state ^{31}P and ^{15}N NMR chemical shift data as well as P–N bond length measurements

in two inhibitors of thermolysin, ZG^{P}LA and ZF^{P}LA, both as free lithium salts and bound to the enzyme. Unexpectedly, we do *not* detect the 1.90-Å P–N bond length in the thermolysin–ZF^{P}LA complex suggested by the crystallographic data (Holden et al., 1987). Instead, we measure similar P–N bond lengths (r_{P-N} = 1.65–1.68 Å) in both free ZF^{P}LA and ZG^{P}LA and when both are bound to the enzyme. Furthermore, we observe only minor movements in the ^{15}N chemical shifts for both inhibitors upon binding. Together with the P–N bond distance measurements, these results indicate that the protonation state of the amide nitrogen does not change in either of the two thermolysin–inhibitor complexes. However, we do observe large changes in ^{31}P chemical shift values upon inhibitor binding, the changes being more pronounced for ZF^{P}LA than for ZG^{P}LA. This indicates that the difference in binding affinity between the two inhibitors is due to structural differences in the neighborhood of the PO_2 group. In particular, the ^{31}P chemical shift data suggest the formation of a bidentate zinc complex between the ZF^{P}LA PO_2 and the protein zinc ion and/or the formation of strong and favorable hydrophobic interactions, as indicated by X-ray crystallographic data (Holden et al., 1987). The latter features are probably responsible for the enhanced affinity of ZF^{P}LA for thermolysin.

Experimental Procedures

Materials. Thermolysin was purchased from Calbiochem and crystallized by the methods of Holmes and Matthews (1982). Approximately 100 mg of thermolysin was crystallized from a 0.05 M Tris acetate buffer at pH 7.5, containing DMSO and cesium chloride, by vapor diffusion against water. After 2–3 weeks, suitable hexagonal crystals were available and were equilibrated in a standard mother liquor containing 0.01 M Tris acetate, 10 mM calcium acetate, and 7% (v/v) DMSO at pH 7.2. The ^{15}N-labeled thermolysin inhibitors ZG^{P}LA and ZF^{P}LA were synthesized with ^{15}N-labeled L-leucine as starting material, by using methods described previously (Bartlett & Marlowe, 1983). For the MAS NMR experiments the thermolysin crystals were transferred into 7-mm aluminum oxide rotors and filled to approximately $^3/_4$ of the rotor's volume of ~300 μL, corresponding to about 150–200 mg of protein. Approximately 1 equiv of either ZG^{P}LA or ZF^{P}LA inhibitor was dissolved in 100–200 μL of standard mother liquor; the inhibitor solution was then layered onto the thermolysin crystals for 2–3 days to allow for diffusion of the inhibitor into the protein crystals. Subsequently, the remaining supernatant was removed from the NMR rotors before acquiring the MAS spectra.

Solid-State NMR Experiments. The ^{15}N and ^{31}P MAS spectra were acquired on a home-built spectrometer, with ^{15}N, ^{13}P, and ^1H Larmor frequencies of 32.2, 128.6, and 317.8 MHz, respectively. In the MAS chemical shift measurements, we employed a home-built, double-resonance, variable-temperature probe with $\pi/2$ ^{15}N, ^{31}P, and ^1H pulse lengths of 4.5, 7.5, and 3.5 μs, respectively. For the P–N bond distance measurements, a variable-temperature triple-resonance MAS probe was constructed (Copié et al., to be published). The $\pi/2$ ^{15}N, ^{31}P, and ^1H pulse lengths for this probe were approximately 5.5, 9.0, and 3.8 μs, respectively. Typical cross-polarization times were 1.5–2 ms, spinning speeds were 2–3 kHz for chemical shift MAS experiments, and recycle delays were 3 s. Both probes employed commercial rotors and stators (Doty Scientific, Columbia, SC).

The two-dimensional XDMR4 experiments were performed at least twice for each P–N bond distance determination, using freshly prepared thermolysin–inhibitor complexes for each enzyme sample. Spectra of the enzyme–inhibitor complexes were recorded at low temperature (−45 to −90 °C), whereas the free inhibitor lithium salts were studied at room temperature. One-dimensional ^{31}P and ^{15}N MAS NMR spectra required about 12–16 h of signal averaging, while each two-dimensional XDMR4 experiment required 64 h of data acquisition at a constant spinning speed and temperature. Stable spinning speeds were achieved by using a spinning speed controller described elsewhere (deGroot et al., 1988).

^{15}N chemical shifts are referenced to external $^{15}NH_4Cl$ and ^{31}P chemical shifts to barium diethyl phosphate (BDEP), which is 5.5 ppm upfield from 85% H_3PO_4 (Herzfeld et al., 1978). No corrections were made for bulk susceptibility effects, which are expected to be small. Chemical shift anisotropies were obtained from an analysis of rotational sideband intensities according to the method of Herzfeld and Berger (1980).

Solution ^{31}P NMR Experiments. ^{31}P solution NMR spectra of the thermolysin–ZG^{P}LA and –ZF^{P}LA complexes were recorded on a 360-MHz spectrometer, with a ^{31}P Larmor frequency of 145.6 MHz. The enzyme–inhibitor liquid samples were prepared in a buffer containing 3 M NaBr, 50 mM Tris, and 10 mM $CaCl_2$ at pH 7.2, according to the method of Gettins (1988). Typical thermolysin protein concentrations were 2.42 mM, and slightly more than 1 equiv of ZG^{P}LA inhibitor was used in preparation of the thermolysin–ZG^{P}LA sample. For the thermolysin–ZF^{P}LA complex, only 0.66 mM inhibitor was used. Samples (3.0 mL) in 10-mm diameter sample tubes were used with 90% H_3O/10% D_2O. ^{31}P sectra were collected with WALTZ ^1H decoupling (Shaka et al., 1983), a 30° phosphorus pulse length of 6.0 μs, and a recycle delay of 1 s. The solution NMR spectra of the thermolysin–inhibitor complexes typically required 40 000 scans with 12 h of data acquisition and were recorded at room temperature. The ^{31}P chemical shifts were measured relative to external 1% TMP in C_6D_6 and to an external 2% ATP solution in D_2O at pH 8.0 which in turn were referenced to 85% H_3PO_4. The α-phosphorus resonance of our ATP solution was taken to be 10 ppm upfield from the 85% H_3PO_4 phosphorus signal.

Results and Discussion

(A) ^{31}P–^{15}N Bond Length Measurements in a Phosphoramidate Model Compound and Thermolysin–Inhibitor Complexes. (1) The XDMR4 Technique. Figure 3 shows the calculated ω_1 projections as a function of r_{P-N}, which was varied from 1.40 to 1.90 Å, with $\omega_r/2\pi$ = 2.0 kHz. Note that the XDMR4 ω_1 projections show dipolar sidebands spaced at $\omega_r/4$, as opposed to spectra from normal MAS which has sidebands spaced at ω_r. The spectral simulations illustrate the manner in which the relative intensities of the first set of dipolar sidebands vary with respect to the intensities of the second and higher order sidebands, as a function of r_{P-N}. In particular, an increase in the P–N bond length results in a decrease in intensity of the second and higher order dipolar sidebands with respect to that of the first. Most importantly, these simulations establish that it is straightforward to distinguish between XDMR4 ω_1 projections corresponding to small changes (<0.1 Å) in r_{P-N}.

The accuracy of the XDMR4 experiment in measuring P–N bond lengths was evaluated by comparing r_{P-N} in diphenyl *N*-methylphosphoramidate, $(PheO)_2PONHCH_3$, measured from the two-dimensional NMR technique with the distance determined by X-ray crystallography. The crystal structure of $(PheO)_2PONHCH_3$ was determined at the single-crystal X-ray diffraction facility at MIT by William M. Davis, and it was found that the P–N bond was short, with r_{P-N} = 1.605 ± 0.002 Å, reflecting some double bond character of the P–N

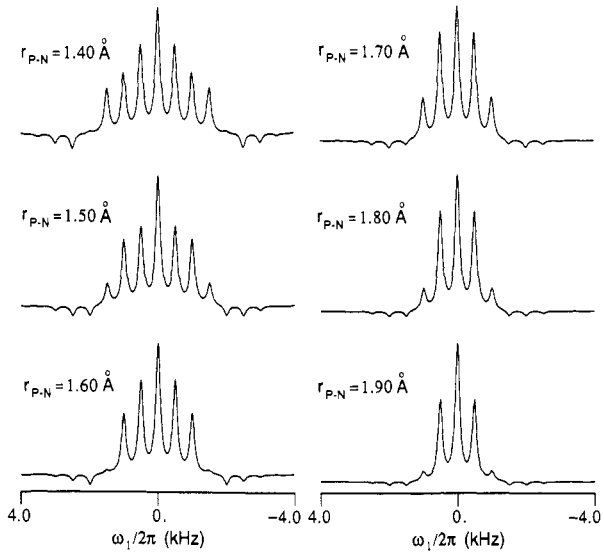

FIGURE 3: Simulated XDMR4 ω_1 projections as a function of r_{P-N} bond distances. These spectral simulations were carried out for a spinning speed $\omega_r/2\pi$ = 2.0 kHz and show dipolar sidebands spaced at 500 Hz. As r_{P-N} increases, the relative intensities of higher order dipolar sidebands decrease. These simulations demonstrate the extreme sensitivity of the technique to the $^{31}P-^{15}N$ bond length.

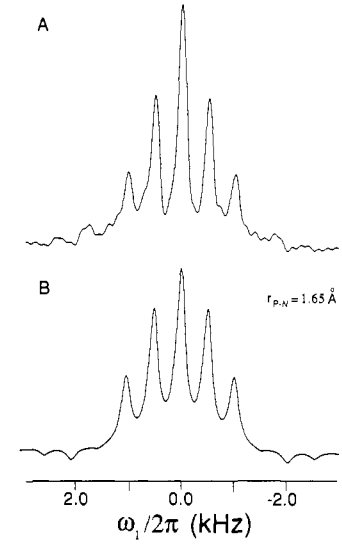

FIGURE 4: XDMR4 ω_1 projection of diphenyl *N*-methylphosphoramidate. (A) Experimental XDMR4 ω_1 projection of $(PheO)_2PONHCH_3$ with $\omega_r/2\pi$ = 2.0 kHz and recycle delay of 60 s. A total of 48 slices were acquired over 12 rotor periods in t_1 with 16 acquisitions per slice. A 175-Hz line broadening was used in the Fourier transformation. (B) Simulated XDMR4 spectrum with r_{P-N} = 1.65 Å. The best fit of the simulation to the spectrum is achieved with a P–N bond length of 1.65 ± 0.02 Å.

linkage (Davis et al., to be published). From fits of the XDMR4 ω_1 projections, we measured, in duplicate NMR experiments, r_{P-N} = 1.65 ± 0.02 Å. Figure 4A shows the XDMR4 ω_1 projection of diphenyl *N*-methylphosphoramidate at a spinning speed $\omega_r/2\pi$ = 2.0 kHz, while Figure 4B shows the XDMR4 simulated spectrum with r_{P-N} = 1.65 Å. The centerband intensities of the *experimental* ω_1 projection spectra, as shown in Figure 4 and below, are more intense than predicted by the corresponding XDMR4 simulations. This discrepancy may be attributed to a combination of natural abundance $^{31}P-^{14}N$ spin pairs and dc offsets which contribute to the intensity of the ω_1 centerband, which is at zero frequency. In any case, as discussed by Gullion and Schaefer (1988, 1989a,b), the centerband intensity in the XDMR4 ω_1 projections is unreliable and is therefore excluded from the fit.

Bond length measurements by two-dimensional dipolar–chemical shift NMR experiments such as XDMR4 have associated with them both statistical and systematic errors. The statistical errors affect the precision of the result, not its accuracy, and are due to the noise in the spectrum. In favorable cases, such as bond length determinations in strongly dipolar coupled spin systems in small molecules, the NMR statistical errors can be as small as ±0.005 Å (Roberts et al., 1987). In contrast, the systematic errors which affect the accuracy of the result, but not its precision, have a variety of sources including crystal packing, errors in the approximation of the system as an isolated I–S spin pair, which lead to shorter bond lengths, and motional averaging of the dipolar coupling, which yields longer bond distances. Systematic errors depend upon the type of nuclei involved in the bond and have only been carefully evaluated for the case of $^{15}N-^{1}H$ (+0.035 Å) (Roberts et al., 1987). Although the exact systematic error has not been determined for $^{31}P-^{15}N$ measurements, the phosphoramidate calibration seems to suggest that it is about +0.05 Å and on the long side of the X-ray value of the bond length. Additional comparisons of diffraction and NMR measurements of $^{31}P-^{15}N$ bonds are required for a proper evaluation of this difference.

(2) $^{31}P-^{15}N$ Bond Lengths in Inhibitors and Thermolysin–Inhibitor Complexes. For the free ZF^{p}LA inhibitor, two measurements of the P–N bond distance yielded r_{P-N} = 1.68 ± 0.02 Å. In the thermolysin–ZF^{p}LA complex, the first measurement gave a P–N bond distance of 1.68 ± 0.03 Å, while the second different enzyme–inhibitor sample yielded a distance of 1.65 ± 0.03 Å.

For the free ZG^{p}LA inhibitor, we measured a P–N bond length of 1.60 ± 0.05 Å in two experiments, a distance that is identical with the P–N bond obtained for ZF^{p}LA within experimental error. In the thermolysin–ZG^{p}LA complex, a P–N bond length of 1.55 ± 0.10 Å was measured for the first data set, and 1.50 ± 0.10 Å for the second. The significantly larger measurement errors for ZG^{p}LA are due to broader NMR resonances which arise from a less crystalline ZG^{p}LA sample than ZF^{p}LA, and which degrade the signal-to-noise ratio of the 2D spectrum. This problem is exacerbated by the constant delay between cross-polarization and detection required for the XDMR4 experiment.

The experimental XDMR4 ω_1 projections of free ZF^{p}LA and thermolysin–ZF^{p}LA complex with $\omega_r/2\pi$ = 2.0 kHz are shown in Figure 5, panels A and B, respectively. For reasons of sensitivity, a minimum number of 4 rotor periods of dipolar evolution were acquired in t_1, for the thermolysin–inhibitor complex and for free ZF^{p}LA. Since the XDMR4 t_1 FID is periodic modulo $4\tau_r$, four rotor periods of acquisition correspond to only a single rotational echo in t_1. Here and below, where this is described, the experimental FID's of the t_1 projections were replicated, using the periodicity of the signal, to artificially increase the resolution. The replication, followed by an exponential filter, disperses the intensity of each point throughout a line shape, facilitating measurement of the line intensities. The simulations were fit to each spectrum by comparing the relative intensities of the first and second sets of dipolar sidebands. The higher order sideband intensities are too close to the estimated noise level (as assessed by the signal-to-noise ratio in the ω_2 dimension) to be reliably taken into consideration. The sidebands seen in the experimental data at higher multiples of $\omega_r/4$ are due to the imposition of a $4\tau_r$ periodicity on the *noise* during replication of the experimental FID. Eliminating the noise-generated sidebands would require exponential broadening of the spectrum to an

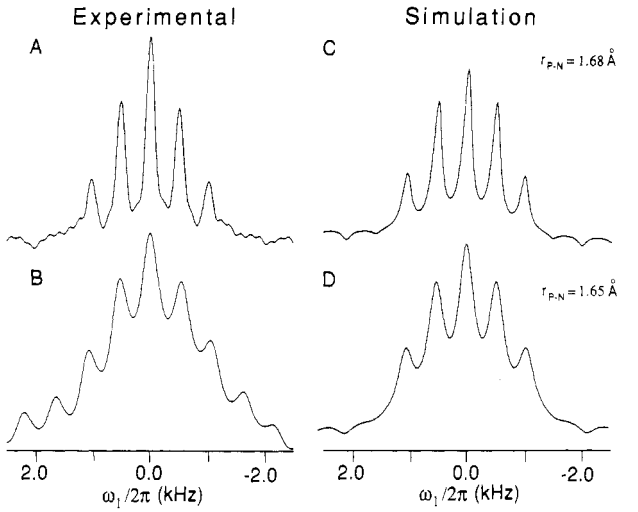

FIGURE 5: XDMR4 ω_1 projections of free ZF^{P}LA inhibitor and thermolysin–ZF^{P}LA complex with $\omega_r/2\pi$ = 2.0 kHz. (A) Experimental XDMR4 ω_1 projection of free ZF^{P}LA inhibitor taken at room temperature, with a recycle delay of 1 s. A total of 48 slices were acquired over 12 rotor periods in t_1 with 1024 acquisitions per slice. A 175-Hz line broadening was used in the Fourier transformation. (B) Experimental XDMR4 ω_1 projection of thermolysin–ZF^{P}LA enzyme–inhibitor complex, taken at an inflow N_2 gas temperature T = −91 °C, with a recycle delay of 3 s. A total of 16 slices were acquired over 4 rotor periods in t_1, with 4800 acquisitions per slice. The t_1 projection was replicated before Fourier transformation, and the spectrum is displayed with 400-Hz line broadening. (C) Simulated XDMR4 ω_1 projection of free ZF^{P}LA with r_{P-N} = 1.68 Å. The best fit to the experimental data is achieved with a P–N bond length of 1.68 ± 0.02 Å. (D) Simulated XDMR4 ω_1 projection of thermolysin–ZF^{P}LA with r_{P-N} = 1.65 Å. The best fit to the experimental spectrum is achieved with a P–N bond length of 1.65 ± 0.03 Å.

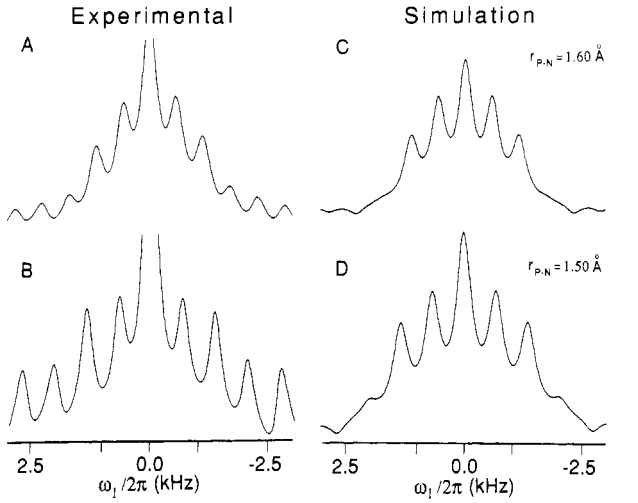

FIGURE 6: XDMR4 ω_1 projections of free ZG^{P}LA inhibitor and thermolysin–ZG^{P}LA complex. (A) Experimental XDMR4 ω_1 projection of free ZG^{P}LA inhibitor taken with $\omega_r/2\pi$ = 2.0 kHz at room temperature and a recycle delay of 3 s. A total of 16 slices were acquired over 4 rotor periods in t_1, with 2240 acquisitions per slice. The t_1 signal was replicated as described in the text. (B) Experimental XDMR4 spectrum of thermolysin–ZG^{P}LA complex, taken at an inflow N_2 gas temperature T = −60 °C, with ω_r = 2.20 kHz and a recycle time of 3 s. A total of 10 slices were acquired over 4 rotor periods in t_1, with 7200 acquisitions per slice. As in the ZG^{P}LA spectrum above, the t_1 signal was replicated and broadened before Fourier transformation. For both experimental spectra described above, a 400-Hz line broadening was used in the Fourier transformations. (C) Simulated XDMR4 spectrum of free ZG^{P}LA with r_{P-N} = 1.60 Å. The best fit to the experimental spectrum is achieved with a P–N bond length of 1.60 ± 0.05 Å. (D) Simulated XDMR4 spectrum of thermolysin–ZG^{P}LA with r_{P-N} = 1.50 Å. The best fit to the data is achieved with a P–N bond length of 1.50 ± 0.10 Å.

extent such that all spectral resolution would be lost, thus defeating the purpose of the replication. It is important to note that these sidebands do not appear in the calculated spectra, although the spectral simulations are replicated and broadened before Fourier transformation in a manner analogous to that of the experimental data. The noise-generated sidebands are larger in the spectra with lower signal-to-noise ratios and therefore are a manifestation of the noise level in ω_1. Consequently, any higher order sideband intensities comparable to these sidebands cannot be reliably incorporated into the determination of r_{P-N}. The best fit to the experimental ZF^{P}LA XDMR4 spectrum is shown in Figure 5C and was achieved with a P–N bond length of 1.68 ± 0.02 Å. The simulated XDMR4 spectrum of thermolysin–ZF^{P}LA is shown in Figure 5D, with the best fit corresponding to a P–N bond length of 1.65 ± 0.03 Å. It should also be noticed that these line shapes and simulations are distinctly different from the 1.90-Å simulation in Figure 3.

Panels A and B of Figure 6 show the experimental XDMR4 ω_1 projections of free ZG^{P}LA inhibitor and thermolysin–ZG^{P}LA, while the best fit simulated XDMR4 spectrum of free ZG^{P}LA is shown in Figure 6C with r_{P-N} = 1.60 ± 0.05 Å. In comparison, the simulated XDMR4 spectrum of thermolysin–ZG^{P}LA is shown in Figure 6D with r_{P-N} = 1.50 Å. Because of a smaller sample volume, the sensitivity is poorer, and the best fit in this case is achieved with a P–N bond length of 1.50 ± 0.10 Å.

As discussed above, there is often some discrepancy between bond distances measured from NMR dipolar couplings and X-ray data (Stoll et al., 1976; Stark et al., 1983; Roberts et al., 1987) which is often attributed to internuclear motion that averages the dipolar coupling. However, in the cases considered here, we are dealing with relatively heavy atoms and therefore expect these effects to be small. Furthermore, all of the experiments were performed at low temperatures (−60 °C) where molecular motion should be significantly reduced. Thus, errors in NMR distance measurements due to motional averaging are likely to be minimal in the thermolysin–ZG^{P}LA and –ZF^{P}LA complexes.

To summarize, the NMR measurements indicate that, within experimental errors, there is no difference in P–N bond length between free ZF^{P}LA and free ZG^{P}LA. Furthermore, we detect no change in bond length as the inhibitors bind to thermolysin. Thus, for both free and bound ZF^{P}LA, we record r_{P-N} = 1.68 ± 0.03 Å, and for free and bound ZG^{P}LA, we find r_{P-N} = 1.60 ± 0.10 Å, yielding an average P–N bond distance for the free and bound forms of both inhibitors of ~1.68 Å. We believe that the apparent P–N bond length difference between ZG^{P}LA and ZF^{P}LA is not real but reflects the fact that the NMR measurements on ZG^{P}LA have larger experimental errors, due to the lower crystallinity of the ZG^{P}LA samples. Nevertheless, the NMR results clearly indicate that the P–N bond distance in the thermolysin–ZF^{P}LA complex is much shorter than the 1.90-Å distance suggested by X-ray crystallography (Holden et al., 1987). These results along with the chemical shift data obtained from the rotational sideband spectra (Herzfeld & Berger, 1980) are compiled in Table I.

(B) ^{31}P Solid-State NMR Chemical Shifts. ZF^{P}LA binding to thermolysin results in a ~20 ppm downfield movement in ^{31}P isotropic chemical shift (σ_{iso}). As seen in Table I, this change in σ_{iso} originates from a 30 ppm downfield shift in the σ_{11} and σ_{22} elements of the chemical shift tensor, whereas σ_{33} remains almost unchanged. Panels A and B of Figure 7 show the 128.6-MHz ^{31}P MAS spectra of free ZF^{P}LA with $\omega_r/2\pi$ = 2.73 kHz, and of thermolysin–ZF^{P}LA complex with $\omega_r/2\pi$ = 2.50 kHz, where the ^{31}P isotropic shifts are positioned at

Table I: ^{15}N and ^{31}P Isotropic Chemical Shifts (σ_{iso}) Derived from Solid-State MAS Spectra and ^{31}P Chemical Shift Tensor Elements (σ_{ii}) Obtained from Rotational Sideband Analysis, as Well as P–N Bond Distances Measured by the XDMR4 NMR Experiments[a]

sample	P–N bond length d (Å)	^{15}N–σ_{iso} (ppm)	^{31}P–σ_{iso} (ppm)	^{31}P chemical shift tensor (ppm)			^{31}P CSA	
				σ_{11}	σ_{22}	σ_{33}	δ (ppm)	η
free ZFPLA	1.68 ± 0.02	12.2	17.9	−53.5	12.5	93.5	76.5	0.69
thermolysin–ZFPLA complex	1.68 ± 0.03	16.3	36.7	−23.5	42.5	90.5	54.0	1.00
free ZGPLA	1.60 ± 0.05	18.0	23.6	−38.9	10.0	99.7	76.2	0.65
thermolysin–ZGPLA complex	1.50 ± 0.10	20.0	28.1	−30.7	20.6	94.5	66.3	0.77

[a] All ^{15}N and ^{31}P chemical shifts are in ppm and referenced to external $^{15}NH_4CL$ and 85% H_3PO_4, respectively. The ^{31}P chemical shifts were measured relative to barium diethyl phosphate (BDEP), which is taken to be 5.5 ppm upfield from 85% H_3PO_4 (Herzfeld et al., 1978). Estimated errors for the σ_{ii} are ±5 and ±0.2 ppm for MAS isotropic shifts. δ and η refer to the chemical shift anisotropy (CSA) and are defined as follows: $\delta = \sigma_{33} - (1/3)\ \mathrm{Tr}\ (\bar{\sigma})$; $\eta = (\sigma_{22} - \sigma_{11})/[\sigma_{33} - (1/3)\ \mathrm{Tr}\ (\bar{\sigma})]$. Quoted errors represent a 95% confidence interval in the data presented.

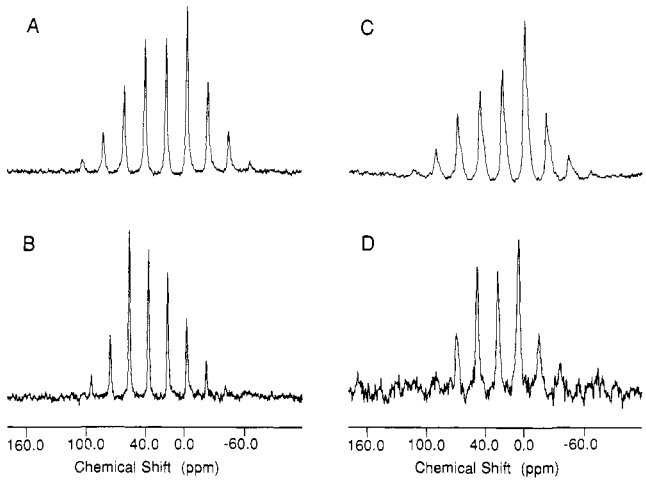

FIGURE 7: 128.6-MHz ^{31}P MAS spectra of ZGPLA and ZFPLA inhibitors and of thermolysin–ZGPLA and –ZFPLA complexes. (A) Free ZFPLA inhibitor at room temperature, with $\omega_r/2\pi$ = 2.73 kHz and a recycle delay of 3 s. The data shown are the Fourier transform of 4800 scans, with ^{31}P isotropic chemical shift resonance at 17.9 ppm. (B) Thermolysin–ZFPLA complex at inflow N_2 gas temperature = −45 °C, $\omega_r/2\pi$ = 2.50 kHz, and recycle delay of 3 s. The Fourier transform is of 14 400 scans, with ^{31}P isotropic chemical shift at 36.7 ppm. (C) Free ZGPLA inhibitor, at room temperature, with $\omega_r/2\pi$ = 3.0 kHz and a recycle delay of 5 s. The Fourier transform is of ~7200 scans, with ^{31}P isotropic chemical shift at 23.6 ppm. (D) Thermolysin–ZGPLA at inflow N_2 gas temperature ~−40 °C, with $\omega_r/2\pi$ = 2.7 kHz and recycle delay of 3 s. The Fourier transform is of 16800 scans, with ^{31}P isotropic resonance at 28.1 ppm. A 50-Hz line broadening was used for Fourier transformation of the FID's except for the thermolysin–ZGPLA sample, where a 100-Hz line broadening was used.

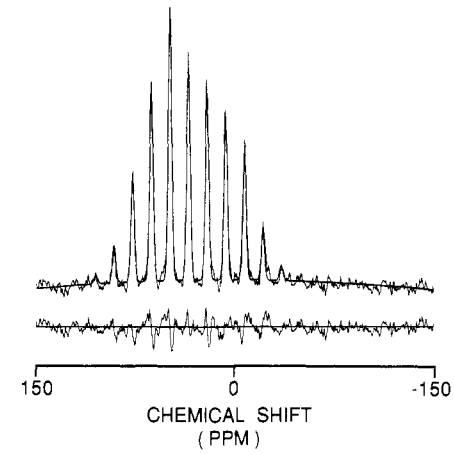

FIGURE 8: Fit of the 128.6-MHz ^{31}P MAS spectrum of thermolysin–ZFPLA complex. Spectral simulation and determination of the principal elements, σ_{11}, σ_{22}, and σ_{33}, of the ^{31}P chemical shift tensor were carried out by analysis of spinning sideband intensities (Herzfeld & Berger, 1980), and by least-squares fitting of the data. The top trace shows the experimental spectrum, with the solid line being the calculated fit. The bottom trace shows the difference between the experimental data and the fit. The sample spinning speed was $\omega_r/2\pi$ = 1.8 kHz, and 19 800 scans were acquired, with a recycle delay of 3 s and a temperature of −52 °C.

17.9 and 36.7 ppm, respectively. Since the protein samples crystallize more readily than the model compounds, the line widths in the thermolysin–ZFPLA spectra are about twice as narrow as observed in the spectra of free ZFPLA lithium salt. Figure 8 shows a ^{31}P MAS spectrum and simulation of thermolysin–ZFPLA complex, taken at a slower spinning speed $\omega_r/2\pi$ = 1.80 kHz and a temperature T = −52 °C. The spectral fit determined the principal elements, σ_{11}, σ_{22}, and σ_{33}, of the chemical shift tensor by rotational sideband intensity analysis (Herzfeld & Berger, 1980). The residuals, data minus fit, are shown in the lower trace.

For ZGPLA, we observe a similar pattern, although the ^{31}P chemical shift changes are not as pronounced. As shown in Table I, a ~5 ppm change in σ_{iso} occurs upon ZGPLA binding to thermolysin. The origin of this movement is a ~10 ppm downfield shift of both σ_{11} and σ_{22}, while again σ_{33} is relatively unaffected. The ^{31}P MAS spectra of the free ZGPLA lithium salt and thermolysin–ZGPLA complex are shown in panels C and D of Figure 7, with ^{31}P isotropic resonances at 23.6 and 28.1 ppm, respectively. The breadth of the ZGPLA ^{31}P NMR resonances, which contributes to the poor sensitivity of the XDMR4 spectra relative to corresponding ZFPLA spectra, is very apparent in the ^{31}P MAS spectrum of free ZGPLA (Figure 7C). Nevertheless, it is interesting to note that the σ_{33} elements for all four samples of free and enzyme-bound ZFPLA and ZGPLA have almost the same value.

Although it is difficult to relate these changes in chemical shift directly to structural changes, they nevertheless indicate that certain features present in the crystallographic structure may be more important than previously supposed. As depicted in Figure 1, the binding of the inhibitors involves the coordination of the Zn^{2+} ion by the $-PO_2-$ group of the inhibitor. In the case of ZFPLA this is primarily a bidentate interaction, while in ZGPLA, the coordination is believed to be monodentate (Holden et al., 1987). Furthermore, the aromatic side chain of ZFPLA forms favorable hydrophobic contacts with the protein, which are absent in the case of ZGPLA. In most structures, these types of interactions lead to shift changes amounting to a few ppm, and therefore the large ~20 ppm effect observed for ZFPLA is surprising. In general, a shift of this magnitude is associated with significant alterations in the covalent bonding. For example, in going from a PO_4 to a CPO_3 (phosphonate) or from CPO_3 to CPO_2C (phosphinate), effects of this size are observed (Emsley, 1966; Gorenstein, 1984). More recently, the ATP-dependent phosphorylation of a phosphinate inhibitor of D-Ala-D-Ala ligase has been shown to produce this size effect (McDermott et al., 1990). While we have absolutely no evidence for a covalent linkage between the phosphonamidate inhibitors and ther-

molysin, the magnitude of the change in ^{31}P chemical shift indicates that the Zn^{2+} complex formation and the steric effects are anomalously strong. It is these interactions that probably contribute to the enhanced affinity of ZFPLA for thermolysin.

Finally, the last entries in Table I are two parameters, δ and η, which describe the ^{31}P chemical shift anisotropy (CSA) for the different thermolysin–inhibitor samples and are related to the chemical shift tensor elements as follows:

$$\delta = \sigma_{33} - (1/3)(\sigma_{11} + \sigma_{22} + \sigma_{33}) \qquad \eta = (\sigma_{22} - \sigma_{11})/\delta$$

Analysis of chemical shift anisotropy parameters has proven to be very useful in assessing the symmetry of electronic distributions, protonation state, hydrogen bonding, or electronic rearrangements around ^{15}N and ^{13}C nuclei and has been applied to the structural elucidation of the retinal chromophore in bacteriorhodopsin (Harbison et al., 1983, 1985a,b). The parameter δ provides an estimate of the departure from spherical symmetry of the electrons around the ^{31}P nucleus (Haeberlen, 1976). In our case, it is interesting to note that the chemical shift anisotropy is much reduced upon ZFPLA binding to thermolysin, δ changing from 76.5 to 54.0 ppm. This means that, upon ZFPLA binding to thermolysin, the electronic distribution around the phosphorus atom becomes more symmetric. This reduction in chemical shift anisotropy could originate from charge neutralization of the PO_2^- by the protein zinc ion and/or by changes in bond angles or distances. The parameter η describes the cylindrical symmetry of the electronic distribution around the ^{31}P nucleus, with $\eta = 0$ representing axial symmetry about σ_{33} (Haeberlen, 1976; Mehring, 1983). As ZFPLA binds to thermolysin, its phosphorus tensor becomes fully axially asymmetric, changing from an $\eta = 0.69$ to an $\eta = 1.00$ tensor. For ZGPLA, the reduction in chemical shift anisotropy upon inhibitor binding is not as pronounced, δ changing from 76.2 to 66.3 ppm and η from 0.65 to 0.77. These data suggest that, for ZGPLA, the structural rearrangements are less pronounced upon binding to thermolysin. This is consistent with a model in which ZGPLA does not form such a tight-binding enzyme complex as ZFPLA, due to less optimal steric interactions and/or to the formation of a monodentate rather than a bidentate complex with the protein zinc ion (Holden et al., 1987). In summary, these changes in δ and η can only be interpreted in a qualitative manner, since the theoretical foundations as to the structural origins of chemical shift changes are still incomplete. Nevertheless, they clearly indicate the presence of a protein-induced electronic symmetrization effect around the phosphorus atom which is more pronounced in ZFPLA than in ZGPLA.

(*C*) *^{15}N NMR Isotropic Chemical Shifts.* The ^{15}N solid-state NMR spectra of thermolysin–ZFPLA and –ZGPLA complexes are shown in Figure 9, panels A and B, respectively, with the ^{15}N isotropic chemical shift resonances at 16.3 ppm for enzyme-bound ZFPLA and at 20.1 ppm for enzyme-bound ZGPLA. The broad resonance at ~82 ppm in both spectra is due to the natural abundance ^{15}N in the peptide backbone. ^{15}N chemical shift anisotropies are small for single-bonded nitrogens and are therefore significantly averaged by even moderate sample rotation rates. For this reason, we were not able to obtain significant sideband intensities and therefore measure the ^{15}N shift anisotropies. However, for both ZGPLA and ZFPLA, the changes in the ^{15}N isotropic chemical shifts (σ_{iso}) are small upon binding to thermolysin, as seen in Table I. Specifically, we observe downfield shifts of 2 and 4 ppm for ZGPLA and ZFPLA, respectively. These results, together with the short P–N bond lengths measured, seem to indicate that the nitrogen atom is not protonated in either ZFPLA– or

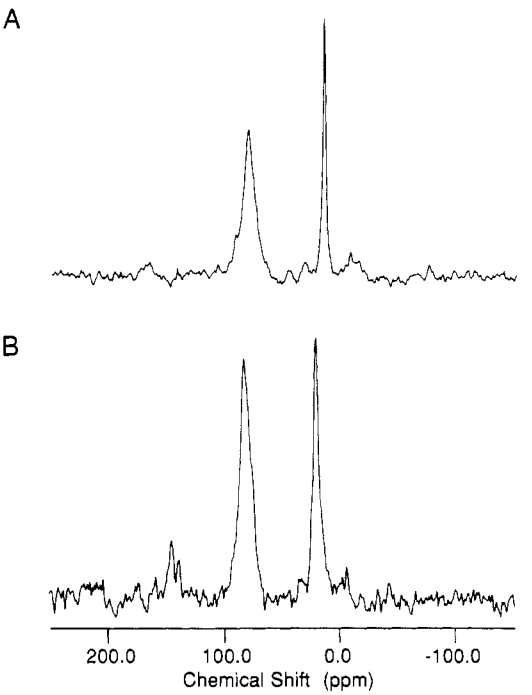

FIGURE 9: 32-MHz ^{15}N MAS spectra of thermolysin–ZFPLA and thermolysin–ZGPLA enzyme–inhibitor complexes at low temperature. (A) Thermolysin–ZFPLA complex, with rotation rate $\omega_r/2\pi = 2.90$ kHz, N_2 gas inflow temperature $T = -40$ °C, and recycle delay of 3 s, and with 24000 scans. The NMR resonance at 81.5 ppm is due to the natural abundance ^{15}N in the peptide backbone, while the line at 16.3 ppm arises from the ^{15}N-labeled ZFPLA inhibitor bound to the enzyme. (B) Thermolysin–ZGPLA complex, with $\omega_r/2\pi = 2.35$ kHz, N_2 gas inflow $T = -37$ °C, and recycle delay of 3 s, and with 19200 scans. The natural abundance ^{15}N signal from the amide backbone nitrogens is at 81.9 ppm, while the ^{15}N ZGPLA enzyme-bound inhibitor resonance appears at 20.1 ppm.

ZGPLA–thermolysin complexes. The ^{15}N NMR results also support the conclusion that changes in P–N bond lengths are *not* responsible for the large ^{31}P chemical shift effects observed in ZFPLA. It also seems unlikely that the ^{31}P NMR changes are due to P–N–C bond angle strains, since these two structural changes are expected to affect the nitrogen as well as the phosphorus resonances.

(*D*) *Solution ^{31}P NMR Chemical Shifts.* The solution ^{31}P NMR spectrum of thermolysin–ZGPLA is shown in Figure 10A and was taken at pH 7.2, the same pH as for the thermolysin crystals, and in 3 M NaBr. The high salt concentration was necessary to solubilize thermolysin (Gettins, 1988). The thermolysin–ZGPLA solution spectrum shows three ^{31}P resonances. The first lies at 29.5 ppm, exhibits a ^{31}P–^{15}N J coupling of ~30 Hz, and corresponds to the enzyme-bound inhibitor. The second resonance is at 19.4 ppm, shows a ^{31}P–^{15}N J coupling of ~12 Hz, and corresponds to free ZGPLA inhibitor. The third ^{31}P line is upfield at 11 ppm, shows no J coupling, and is assigned to hydrolyzed inhibitor. The enzyme-bound ZGPLA inhibitor ^{31}P isotropic chemical shift in solution is very similar to that found in crystals, indicating that the conformation of the protein's active site in solution is very similar to that present in thermolysin crystals. In contrast, the free ZGPLA inhibitor has a different isotropic ^{31}P chemical shift in solution than in the solid sample (19 ppm vs ~24 ppm). This reflects the molecular packing constraints present for the small inhibitor in its crystal form, as well as the effect of the high NaBr salt concentration on ^{31}P chemical shifts.

The ^{31}P solution NMR spectrum of thermolysin–ZFPLA in Figure 10B shows the relatively broad ^{31}P resonance of the

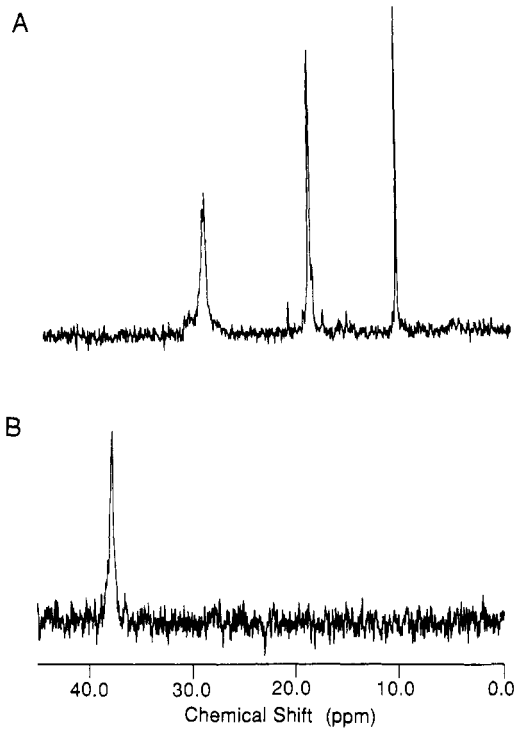

FIGURE 10: 145.6-MHz ^{31}P solution NMR spectra of thermolysin–ZG^{P}LA and thermolysin–ZF^{P}LA enzyme–inhibitor complexes. (A) 2.42 mM thermolysin in the presence of 3.5 mM ZG^{P}LA, with 4020 scans. The broad enzyme-bound inhibitor ^{31}P resonance is located at 29.5 ppm and shows a J coupling of 30 Hz to the ^{15}N nitrogen. The free ZG^{P}LA ^{31}P resonance is at 19.4 ppm and shows a J coupling to ^{15}N of 12.2 Hz. The most upfield resonance at 11.0 ppm is from hydrolyzed, unreacted inhibitor and shows no J coupling. (B) 2.42 mM thermolysin in the presence of 0.66 mM ZF^{P}LA, with 31 196 scans. The only ^{31}P resonance visible is from the enzyme-bound ZF^{P}LA inhibitor and is at 37.8 ppm for 85% H_3PO_4, used as external phosphorus reference chemical shift. The 3-mL samples were prepared in a 90% H_2O/10% D_2O buffer containing 3 M NaBr, 50 mM Tris, and 10 mM $CaCl_2$ at pH 7.2. Both spectra were recorded at room temperature, with a 30° tip pulse of 6 μs and a recycle delay of 1 s. A 30° instead of a 90° tip pulse was used in conjunction with a short recycle time to maximize the signal-to-noise gain over the 12-h data acquisition period. Three- and five-hertz line broadenings were used in the Fourier transforms of the thermolysin–ZG^{P}LA and –ZF^{P}LA spectra, respectively.

enzyme-bound ZF^{P}LA inhibitor at 37.8 ppm and is very close to the value of 36.7 ppm in the crystals. It is interesting to note that salt concentration or molecular crystal packing effects cause much smaller ^{31}P changes than the large 20 ppm downfield shift seen when ZF^{P}LA binds to thermolysin. These solution NMR results eliminate the possibility that the large downfield movement of the ZF^{P}LA ^{31}P resonance seen in the solid-state NMR experiment is due to crystal packing effects. No ^{31}P signals corresponding to free ZF^{P}LA inhibitor or to hydrolyzed ZF^{P}LA are seen in the solution NMR spectrum of thermolysin–ZF^{P}LA, because excess inhibitor was not added to the enzyme during the sample preparation.

Conclusion

Using two-dimensional solid-state NMR techniques, we have measured the ^{31}P–^{15}N bond distances in two thermolysin–ZG^{P}LA and –ZF^{P}LA enzyme–inhibitor complexes. The results indicate that the P–N bond lengths do not increase upon enzyme–inhibitor complex formation and that, within experimental errors, the two inhibitors have a similar P–N bond distance of r_{P-N} = 1.68 Å. For ZF^{P}LA bound to thermolysin, this corresponds to a considerably shorter P–N bond than indicated by X-ray measurements (Holden et al., 1987).

A second feature suggested by the X-ray investigation, protonation of the ^{15}N (Holden et al., 1987), is also inconsistent with the ^{15}N NMR chemical shift results. In particular, protonation should lead to substantial changes in ^{15}N isotropic shifts, and only 2–4 ppm movements are observed.

However, we do observe large perturbations in the ^{31}P shifts of the inhibitors upon binding to the enzyme. The ^{31}P resonance of ZF^{P}LA moves ~20 ppm downfield in both crystals and solution, upon complex formation with thermolysin. In ZG^{P}LA, inhibitor binding results in a ^{31}P chemical shift change of approximately 5 ppm. These results are consistent in part with the X-ray crystallographic model, which proposes that the difference in binding constants between ZF^{P}LA and ZG^{P}LA resides in differential interactions between the protein, its zinc metal ion, and the inhibitor $^{31}PO_2$ functional group.

Finally, the experiments described here represent another example of the utility of solid-state NMR in elucidating enzyme–inhibitor structures. With the availability of sufficient quantities of enzyme, both heteronuclear and homonuclear distances may be determined in polycrystalline samples with good accuracy, and with precision equal to or better than that of diffraction techniques (Raleigh et al., 1988, 1989). These approaches should find increasing application in the study of a number of problems in structural biochemistry.

Acknowledgments

We are particularly grateful to Mr. Peter Allen for his invaluable technical assistance in constructing the variable-temperature triple resonance probe and to Dr. Ann McDermott for her enthusiastic and critical comments regarding this work.

References

Abragam, A. (1961) *Principles of Nuclear Magnetism*, p 122, Oxford University Press, London.

Bartlett, P. A., & Marlowe, C. K. (1983) *Biochemistry 22*, 4618–4624.

Bartlett, P. A., & Marlowe, C. K. (1987a) *Biochemistry 26*, 8553–8561.

Bartlett, P. A., & Marlowe, C. K. (1987b) *Science 235*, 569–571.

Bolognesi, M. C., & Matthews, B. W. (1979) *J. Biol. Chem. 254*, 634–639.

deGroot, G. J. M., Copiê, V., Smith, S. O., Allen, P. J., Winkel, C., Lugtenburg, J., Herzfeld, J., & Griffin, R. G. (1988) *J. Magn. Reson. 77*, 251–257.

Ehlers, M. R. W., & Riordan, J. F. (1989) *Biochemistry 28*, 5311–5318.

Emsley, J. W., Feeney, J., & Sutcliffe, L. H. (1966) *High Resolution Nuclear Magnetic Resonance Spectroscopy*, Vol. 2, Pergamon Press, Oxford.

Endo, S. (1962) *J. Ferment. Technol. 40*, 346.

Erdos, E. G., & Skidgel, R. A. (1989) *FASEB J. 3*, 145–151.

Fersht, A. R. (1984) *Enzyme Structure and Mechanism*, 2nd ed., W. H. Freeman and Co., New York.

Fournie-Zaluski, M. C. (1988) *Neurochem. Int. 12*, 375–382.

Gettins, P. (1988) *J. Biol. Chem. 263*, 10208–10211.

Gorenstein, D. G. (1984) *Phosphorus–31 NMR: Principles and Applications* (Gorenstein, D., Ed.) Academic Press, Orlando, FL.

Gullion, T., & Schaefer, J. (1989a) *J. Magn. Reson. 81*, 196–200.

Gullion, T., & Schaefer, J. (1989b) *Adv. Magn. Reson.* (in press).

Gullion, T., Poliks, M. D., & Schaefer, J. (1988) *J. Magn. Reson. 80*, 553–558.

Haeberlen, U. (1976) *High-Resolution NMR in Solids*, pp 5–15, Academic Press, London.
Hangauer, D. G., Monzingo, A. F., & Matthews, B. W. (1984) *Biochemistry 23*, 5730–5741.
Harbison, G. S., Herzfeld, J., & Griffin, R. G. (1983) *Biochemistry 22* 1–5.
Harbison, G. S., Smith, S. O., Pardoen, J. A., Courtin, J. M. L., Lugtenburg, J., Herzfeld, J., Mathies, R. A., & Griffin, R. G. (1985a) *Biochemistry 24*, 6955–6962.
Harbison, G. S., Mulder, P. P. J., Pardoen, H., Lugtenburg, J., Herzfeld, J., & Griffin, R. G. (1985b) *J. Am. Chem. Soc. 107*, 4809–4816.
Haslanger, M. F., Sybertz, E. J., Neustadt, B. R., Smith, E. M., Nechuta, T. L., & Berger, J. (1989) *J. Med. Chem. 32*, 737–739.
Herzfeld, J., & Berger, A. E. (1980) *J. Chem. Phys. 73*, 6021–6030.
Herzfeld, J., Griffin, R. G., & Haberkorn, R. A. (1978) *Biochemistry 17*, 2711–2718.
Holden, H. M., & Matthews, B. W. (1988) *J. Biol. Chem. 263*, 3256–3260.
Holden, H. M., Tronrud, D. E., Monzingo, A. F., Weaver, L. H., & Matthews, B. W. (1987) *Biochemistry 26*, 8642–8553.
Holmes, M. A., & Matthews, B. W. (1981) *Biochemistry 20*, 6912–6920.
Holmes, M. A., & Matthews, B. W. (1982) *J. Mol. Biol. 160*, 623–639.
Holmes, M. A., Tronrud, D. E., & Matthews, B. W. (1983) *Biochemistry 22*, 236–240.
Holmquist, B., & Vallee, B. (1974) *J. Biol. Chem. 249*, 4601–4607.
Jencks, W. P. (1975) *Adv. Enzymol. Relat. Areas Mol. Biol. 43*, 219–410.
Jencks, W. P. (1980) *Mol. Biol. Biochem. Biophys. 32*, 3–25.
Jencks, W. P. (1981) *Proc. Natl. Acad. Sci. U.S.A. 78*, 4046–4050.
Jencks, W. P. (1987) *Catalysis in Chemistry and Enzymology*, Dover Publications, New York.
Johnson, W. H., Roberts, N. A., & Borkakoti, N. J. (1987) *J. Enzyme Inhib. 2*, 1–22.
Kester, W. R. & Matthews, B. W. (1977) *Biochemistry 16*, 2506–2516.
Kolbert, A. C., Raleigh, D. P., Levitt, M. H., & Griffin, R. G. (1989) *J. Chem. Phys. 90*, 679–689.
Levitt, M. H., Oas, T. G., & Griffin, R. G. (1988) *Isr. J. Chem. 28*, 271.
McDermott, A. E., Creuzet, F., Griffin, R. G., Zawadzke, L. E., Ye, Q.-Z., & Walsh, C. T. (1990) *Biochemistry 29*, 5767–5775.
Mehring, M. (1983) *Principles of High Resolution NMR in Solids*, 2nd ed., pp 40–50, Springer-Verlag, New York.
Monzingo, A. F., & Matthews, B. W. (1984) *Biochemistry 23*, 5724–5729.
Munowitz, M. G., & Griffin, R. G. (1982) *J. Chem. Phys. 76*, 2848. C
Munowitz, M. G., Griffin, R. G., Bodenhausen, G., & Huang, T. H. (1981) *J. Am. Chem. Soc. 103*, 2529–2533.
Oas, T. G., Griffin, R. G., & Levitt, M. H. (1988) *J. Chem. Phys. 89*, 692.
Olejniczak, E. T., Vega, S., & Griffin, R. G. (1984) *J. Chem. Phys. 81*, 4804–4817.
Pauling, L. (1946) *Chem. Eng. News 24*, 1375–1377.
Pines, A., Gibby, M. G., & Waugh, J. S. (1973) *J. Chem. Phys. 59*, 569–590.
Raleigh, D. P., Levitt, M. H., & Griffin, R. G. (1988) *Chem. Phys. Lett. 146*, 71–76.
Raleigh, D. P., Creuzet, F., Das Gupta, S. K., Levitt, M. H., & Griffin, R. G. (1989) *J. Am. Chem. Soc. 111*, 4502–4503.
Robert, J. E., Harbison, G. S., Munowitz, M. G., Herzfeld, J., & Griffin, R. G. (1987) *J. Am. Chem. Soc. 109*, 4163–4169.
Schaefer, J., Stejskal, E. O., & Buchdahl, R. (1975) *Macromolecules 8*, 291.
Seymour, A. A., Swerdal, J. N., Fennell, S. A., Druckman, S. P., Neubeck, R., & Delaney, N. G. (1989) *J. Cardiovasc. Pharmacol. 14*, 194–204.
Shaka, A. J., Keeler, J., Frenkiel, T., & Freeman, R. (1983) *J. Magn. Reson. 52*, 335–338.
Stark, R. E., Jelinski, L. W., Ruben, D. J., Torchia, D. A., & Griffin, R. G. (1983) *J. Magn. Reson. 55*, 266.
Stoll, M. E., Vega, A. J., & Vaughan, R. W. (1976) *J. Chem. Phys. 65*, 4093.
Tronrud, D. E., Monzingo, A. F., & Matthews, B. W. (1986) *Eur. J. Biochem. 157*, 261–268.
Tronrud, D. E., Holden, H. M., & Matthews, B. W. (1987) *Science 235*, 571–574.
Weaver, L. H., Kester, W. R., & Matthews, B. W. (1977) *J. Mol. Biol. 114*, 119–132.
Wolfenden, R. (1976) *Annu. Rev. Biophys. Bioeng. 5*, 271–306.
Wolfenden, R., & Frick, L. (1987) in *Enzyme Mechanisms* (Page, M. I., & Williams, A., Eds.) pp 97–122, Royal Society of Chemistry, Burlington House, London.